Progress in Natural Science: Materials International 27 (2017) 606–614

HOSTED BY

Contents lists available at ScienceDirect

Progress in Natural Science: Materials International

journal homepage: www.elsevier.com/locate/pnsmi

Original Research

Enhanced performance of nano-sized SiC reinforced Al metal matrix nanocomposites synthesized through microwave sintering and hot extrusion techniques

M. Penchal Reddy[a], R.A. Shakoor[a,*], Gururaj Parande[b], Vyasaraj Manakari[b], F. Ubaid[a], A.M.A. Mohamed[c], Manoj Gupta[b]

[a] Center for Advanced Materials, Qatar University, Doha, Qatar
[b] Department of Mechanical Engineering, National University of Singapore, Singapore
[c] Department of Metallurgical and Materials Engineering, Suez University, Suez, Egypt

ARTICLE INFO

Keywords:
Al-SiC nanocomposites
Microwave sintering
Hot extrusion
Mechanical properties
Thermal expansion

ABSTRACT

In the present study, nano-sized SiC (0, 0.3, 0.5, 1.0 and 1.5 vol%) reinforced aluminum (Al) metal matrix composites were fabricated by microwave sintering and hot extrusion techniques. The structural (XRD, SEM), mechanical (nanoindentation, compression, tensile) and thermal properties (co-efficient of thermal expansion-CTE) of the developed Al-SiC nanocomposites were studied. The SEM/EDS mapping images show a homogeneous distribution of SiC nanoparticles into the Al matrix. A significant increase in the strength (compressive and tensile) of the Al-SiC nanocomposites with the addition of SiC content is observed. However, it is noticed that the ductility of Al-SiC nanocomposites decreases with increasing volume fraction of SiC. The thermal analysis indicates that CTE of Al-SiC nanocomposites decreases with the progressive addition of hard SiC nanoparticles. Overall, hot extruded Al 1.5 vol% SiC nanocomposites exhibited the best mechanical and thermal performance as compared to the other developed Al-SiC nanocomposites.

1. Introduction

The development of metal-ceramic matrix composites (MMCs) is of great interest in automobile and aerospace applications due to their potential to exhibit excellent combination of properties such as toughness, ductility, high modulus, corrosion resistance and high strength [1,2]. In MMCs, aluminum based metal matrix composites are being increasingly used in automobiles, aerospace, defense and military industries due to their low density, high specific modulus, high strength to weight ratio and toughness [3–6].

Aluminum is used in a variety of applications due to its high strength to weight ratio but the major drawback is its poor wear resistance. This has been rectified by the addition of hard SiC [7] particles as reinforcement. Addition of SiC ceramic nanoparticles in aluminum, an addition, also leads to improvements in strength, hardness and corrosion resistance. The major advantage of using nanoreinforcements is that the superior properties can be attained at lower volume fractions (< 2%), whereas for micron-scale particles reinforced MMCs higher volume fractions (≫ 10%) are required [8].

Aluminum-silicon carbide (Al-SiC) composites have been considered as promising materials for lightweight structural applications due to their unique combination of low density and high strength. However, in order to produce sound nanocomposites with enhanced mechanical properties, good dispersion of the nanoreinforcement phase within the matrix is necessary, which is in turn strongly governed by the selection of a suitable production process [9–11]. Several processing methods have been developed to prepare Al-SiC composites such as powder metallurgy [12], conventional casting [13], spark plasma sintering [14] and conventional hot extrusion [15].

Generally, powder metallurgy (PM) process is well known to be one of excellent metal synthesis techniques for producing near net shape products. In addition, the undesirable levels of interaction between matrix and reinforcements can be avoided because of lower processing temperatures usually associated with PM methods [3]. New sintering routes such as laser, spark plasma, and microwave sintering (MWS) could offer more advantages in terms of time and energy saving when compared to conventional heating [16]. Among different sintering methods, MWS offers high heating rate, shorter processing time, homogeneous microstructure, improved quality of the product, improved mechanical properties, and environmental friendliness over

Peer review under responsibility of Chinese Materials Research Society.
* Corresponding author.
E-mail address: shakoor@qu.edu.qa (R.A. Shakoor).

http://dx.doi.org/10.1016/j.pnsc.2017.08.015
Received 26 January 2017; Received in revised form 2 August 2017; Accepted 21 August 2017
Available online 30 September 2017

conventional sintering processes [17].

Processing of fine-grained metal matrix composites via microwave sintering was emphasized also, because the consolidation can be achieved at much lower temperatures. The composites obtained through MWS technique can be subjected to secondary processing such as forging, rolling and extrusion. These secondary treatments reduce the porosity, enhance the particle distribution and improve the mechanical properties [18–20].

Microwave processing of powder metallurgy metal composites is a novel integrated manufacturing method that is very rarely seen in recent research works. This research work has done to check the feasibility of synthesis and characterization of the composites by using this novel sintering process [17]. The present work attempts to synthesis Al-SiC nanocomposites via high energy ball milling and microwave sintering process followed by hot extrusion in order to produce high strength composite materials. The structure, microstructure, thermal and mechanical behavior; including the compression strength, tensile strength, ductility and hardness, of the extruded Al-SiC nanocomposites are critically investigated and interrelated.

2. Materials and methods

2.1. Materials

In the present study, pure aluminum powder of the size range ~ 7–15 μm and 99% purity was procured from Alfa Aesar, USA and SiC powder with an average size of ~ 15 nm and purity > 99 +% supplied by nanostructured and amorphous materials, Inc. (Houston, TX, USA), was used as the reinforcement phase for the synthesis of Al-SiC nanocomposites.

2.2. Fabrication of Al-SiC nanocomposites

2.2.1. Primary processing

To produce Al-SiC nanocomposites, nano-sized SiC powder (0.3, 0.5, 1.0 and 1.5 vol%) was added to pure Al. The mixture of powders was blended at room temperature using a Retsch PM400 planetary ball mill for 2 h with the milling speed of 200 rpm in order to get a homogeneous particle distribution. No balls were used in this stage. The blended powder mixture was compacted at a pressure of 97 bar (50 t) into billets of size 35 mm in diameter and 40 mm in length. The consolidated composite specimens are shown in Fig. 1. The compacted cylindrical billets were sintered using an innovative hybrid microwave assisted two-directional sintering technique [21] to achieve a temperature of 550 °C, just below the melting temperature of Al.

2.2.2. Secondary processing

Prior to hot extrusion, the microwave sintered billets were soaked in a resistance furnace at a temperature of 400 °C for 1 h, and then hot extruded at 350 °C under 500 MPa. The extrusion ratio was ~ 20.25:1 to produce an extruded rod with 8 mm diameter (Fig. 1). Colloidal graphite was used as lubricant. These extruded rods were subsequently used for characterization studies.

2.3. Materials characterization

The phase identification of the extruded samples was carried out using X-ray powder diffractometer (PANalytical X'pert Pro) based on Cu-K_α radiation (1.541 Å) over the 2θ range 30–90° at scan rate of 0.2°/min. Individual phases were identified by matching the characteristic XRD peaks against JCPDS data. Field emission scanning electron microscopy (JEOL JSM-6010 and Hitachi FESEM-S4300) equipped with energy dispersion spectroscopy (EDS) was used to identify the reinforcement phase and microstructure of the extruded composite samples.

The hardness of the pure Al and composite samples was determined

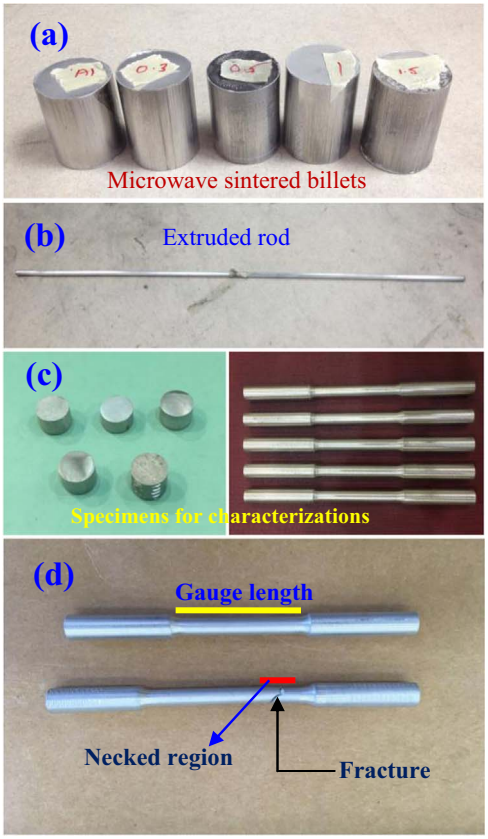

Fig. 1. Samples of Al-SiC nanocomposites: (a) microwave sintered billets, (b) hot extruded rod, (c) machined samples for characterization and (d) failed specimen under tensile loading.

using Vicker's microhardness tester (FM-ARS9000, USA) with applied load of 100 gf for 15 s as per the ASTM standard E384-08. Compressive testing of the cylindrical specimens was performed at room temperature in accordance with the procedures outlined in ASTM standard E9-89a using Universal testing machine-Lloyd. The test specimens with a length to diameter (l/d) ratio ~ 1 were subjected to a compression load at a constant strain rate of 8.3×10^{-4} s^{-1}. From the load-displacement curves, 0.2% offset compressive yield strength (CYS), ultimate compression strength (UCS) and failure strain were determined. Tensile properties of the extruded samples were determined using an universal testing machine-Lloyd in accordance with the ASTM E8/E8M-15a standard at room temperature under the strain rate of 8.3×10^{-4} s^{-1}. The tensile test specimens were smooth round specimens of 5 mm gauge diameter and 25 mm gauge length using a fully automated servo-hydraulic mechanical testing machine, MTS-810. For each composition, three samples were tested to ensure repeatable values. From the stress-strain curves, 0.2% tensile yield strength (TYS), ultimate tensile strength (UTS) and percentage elongation (ductility) were determined. The fracture surfaces of the selected compression and tensile specimens were examined by scanning electron microscope (Hitachi FESEM-S4300). Nanoindentation analysis was performed using a MFP-3D NanoIndenter (head connected to AFM equipment) system equipped with standard Berkovich diamond indenter tip. The testing was performed at room temperature. The hardness (H) and young's modulus (E) in nanoindentation test are directly obtained. The indentation was made to a maximum load of about 100 mN and under loading and unloading rate of 200 μN/s and dwell time at maximum load: 5 s. In order to take the repeatability into account, the test results were acquired from the average of 6 indentations.

Coefficient of thermal expansion of Al-SiC nanocomposites was determined using a INSEIS TMA PT 1000LT thermo-mechanical analyzer. A heating rate of 5 °C/min for a temperature range of 50–

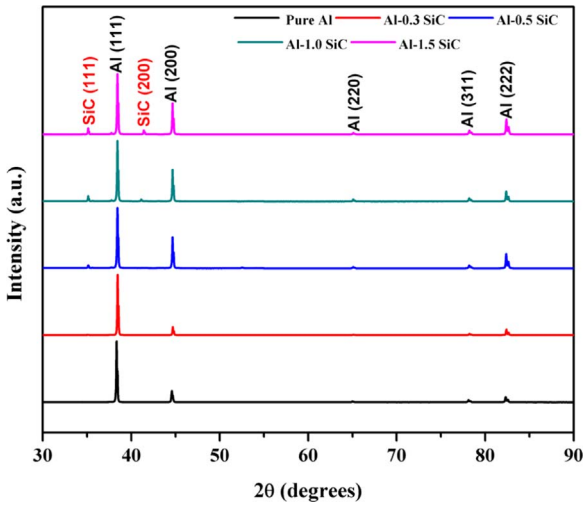

Fig. 2. XRD patterns of microwave-hot extruded Al-SiC nanocomposites.

350 °C with a argon flow rate of 0.1 lpm.

3. Results and discussion

3.1. Phase identification of extruded Al-SiC nanocomposites

The XRD patterns of extruded pure Al and Al-SiC nanocomposites are shown in Fig. 2. During the microwave sintering and hot extrusion process, it is noted that no solid-state reaction took place between the matrix and reinforcement to form any other undesired phases. XRD spectra show no signs of any presence of secondary phases. Similar observations were reported by Omyma et al. [11] for the conventionally extruded Al-SiC composites. The peak of SiC particles is clearly visible in the XRD pattern for the high-volume fraction of SiC reinforcement. However, the absence of SiC peaks in the XRD spectra of Al 0.3 vol% SiC composites can be due to the addition of lower amounts of SiC nanoparticles which are not captured in the XRD spectra. The intensities of SiC peaks are apparently increasing with increasing vol % of SiC nanoparticles. The XRD results reveal that main elements present are Al (largest peak) and SiC (shorter peak). The XRD results also confirm the elemental map results which verify that fabricated composites are SiC reinforced Al-composites.

3.2. Microstructural characterization of extruded Al-SiC nanocomposites

The microstructure of the extruded pure Al and Al-SiC nanocomposites was investigated by SEM and the corresponding micrographs taken from the cross-section of the samples are shown in Fig. 3. A certain degree of clustering of SiC nanoparticles can be observed in the Al matrix which may be attributed to the density difference between the matrix phase (2.7 g/cm^3) and reinforcement phase (3.21 g/cm^3). The tendency of agglomeration at higher volume fractions of reinforcement arises because of the large difference in the sizes of Al powder and SiC powder particles. The nano-size powders tend to fill in the interstitial spaces between the aluminum powders during mixing and compaction. Secondary processing conditions (extrusion) were not sufficient to break the clusters completely and disperse the nanopowder in the metal matrix. Previous studies have reported that agglomeration of SiC particles in Al matrix resulted in the degradation of mechanical properties, as reinforcement clustering along with voids in the particles acted as pre-existing cracks, limiting the stress transfer from the soft matrix to the hard reinforcements during deformation [22,23]. However, these agglomerated sites are only observed at few locations across the matrix and a near-uniform nanoparticle distribution is

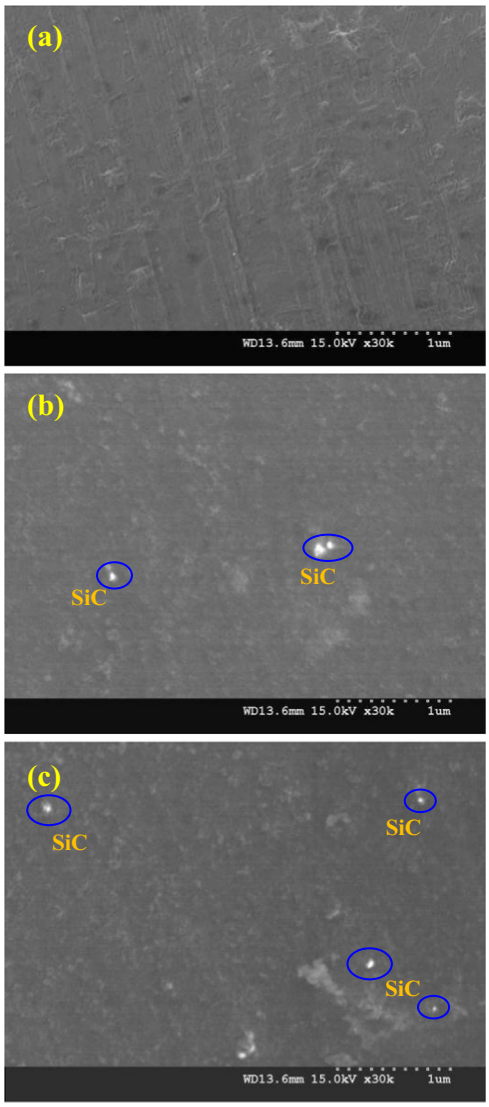

Fig. 3. SEM micrographs of microwave-hot extruded of (a) pure Al, (b) Al-0.5 vol% SiC and (c) Al-1.0 vol% SiC nanocomposites.

noticed in the Al-SiC composite samples. This near-uniform distribution of nanoparticles promotes more even heating throughout the compacted specimens during sintering and demonstrates the effectiveness of using powder metallurgy coupled with hybrid microwave sintering for the synthesis of Al-based nanocomposites [24].

Energy dispersive X-ray spectrometry (EDS) was employed to identify elemental distribution in the Al matrix. The EDX spectrum (Fig. 4a) of the Al-1.5 vol% SiC composite showed that the composite was composed mainly of Al, Si and C elements. Fig. 4(b) represents the microstructure and the corresponding Al, Si, and C composition maps of the extruded composite containing 1.5 vol% of SiC nanoparticles. The elemental distribution map evidently reveals the uniform distribution of SiC nanoparticles in Al matrix and confirms the presence of aluminum and SiC phases.

3.3. Mechanical properties of extruded Al-SiC nanocomposites

The size and amount of reinforcement, type of processing technique and the matrix/particle integrity greatly influence the mechanical properties of an Al-based composite [25,26]. Strong matrix/particle interface integrity was obtained in this study. Therefore, SiC particle volume fraction and the effect of hot extrusion as a secondary processing play an active role in realizing the mechanical properties

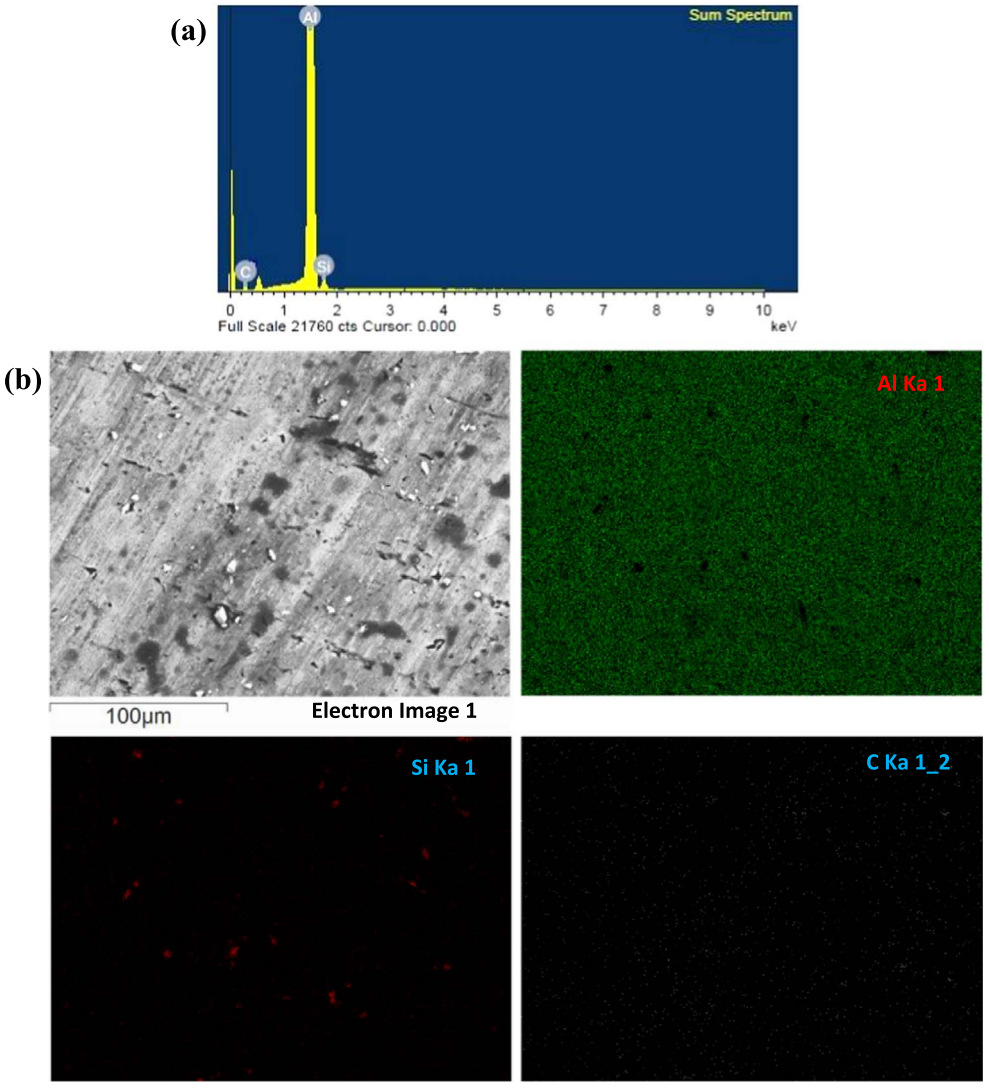

Fig. 4. EDS spectrum (a) and mapping (b) analysis of microwave-hot extruded Al-1.5 vol% SiC nanocomposite.

of the composites.

3.3.1. Microhardness studies

The microhardness is a very useful important property that reflect the strength and tribological properties of the material. Generally, several factors would affect the microhardness of the composites such as particle size, volume percent, distribution of reinforcement phase, method of preparation and density of the reinforcement [27]. The average microhardness values of the extruded pure Al and Al-SiC composite samples are presented in Fig. 5 and Table 1. The presence of hard SiC particles increases the microhardness of the composites as explained by the rule of mixtures [28].

$$H_c = H_m F_m + H_r F_r \quad (1)$$

where, H_c, H_m and H_r are the hardness of the composite, matrix, and reinforcement, and F_m and F_r are the volume fraction of matrix and reinforcement, respectively.

The increase in hardness of Al-SiC nanocomposites when compared to pure Al can also be attributed to good interface between the soft phase of pure Al and hard phase of SiC formed during milling and a homogenous distribution of the SiC particles in the Al matrix. As the volume fraction of silicon carbide in the composite increases, the hardness value increases, achieving a value of over 82.34 Hv for the Al-1.5 vol% SiC composite, which is consistent with the spark plasma sintered Al-SiC composites [9]. The increase in hardness values with

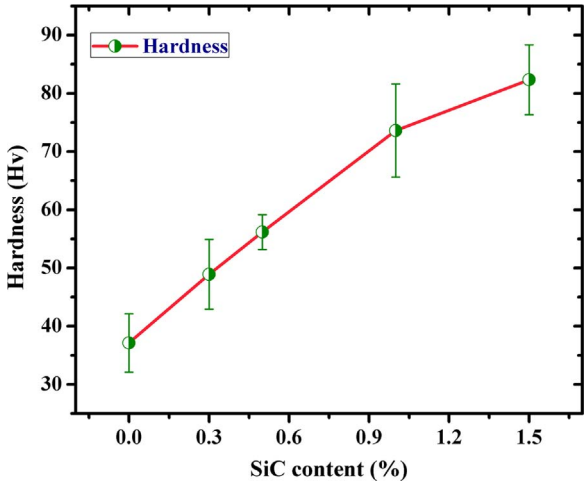

Fig. 5. The variation of hardness of microwave-hot extruded Al-SiC nanocomposites.

the increase in SiC particles can be attributed to the increased presence of hard SiC particles and its constraint towards localized plastic deformation coupled with good matrix-reinforcement interfacial integrity. Similar outcomes of increasing hardness with increasing amount of reinforcement in the matrix irrespective of the fabrication process of

Table 1
Summary of microhardness of Al–SiC nanocomposites produced by different techniques.

S.No	Material	Hardness (Hv)	Method of Preparation	Ref.
1	Pure Al	37 ± 5	Mechanically alloying	
	Al–0.3vol%SiC	49 ± 6	+	
	Al–0.5vol%SiC	56 ± 3	Microwave sintering	[Present study]
	Al–1.0vol%SiC	73 ± 4	+	
	Al–1.5vol%SiC	82 ± 4	Hot Extrusion	
2	Al–20 vol%SiC	74.80		
	Al–25 vol%SiC	81.20	Spark plasma sintering	[9]
3	Pure Al	30.00		
	Al–15 wt%SiC	43.00	Conventional	[10]
	Al–25 wt%SiC	59.00	casting	
4	Pure Al	40.30	Ball milling	
	Al–5 wt%SiC	61.00	+	[11]
	Al–10 wt%SiC	72.00	Hot extrusion	
5	Pure Al	24.50		
	Al–5 wt%SiC	38.67		
	Al–10 wt%SiC	42.30	Stir casting process	[30]
	Al–20 wt%SiC	45.40		

AMMCs were reported by previous researchers [9–11,29,30]. The microhardness values of the microwave-extruded samples are higher than those of the conventional or stir casting samples.

3.3.2. Compressive studies

The room temperature engineering stress-strain curves of the microwave sintered and hot extruded pure Al and Al-SiC nanocomposites under compression loading are shown in Fig. 6(a). The average compressive yield strength (CYS) and ultimate compressive strength (UCS) values of the extruded composites as a function of added SiC particles are shown in Fig. 6(b) and Table 2. Al-1.5 SiC nanocomposite exhibited a compressive strength of 392.16 MPa and yield strength of about 118.9 MPa. According to Fig. 6(b), the compressive strength and yield strength of extruded composites increases with increasing volume percent of nano-sized reinforcement particles. This significant improvement in compression strength properties of the extruded Al-SiC nanocomposites compared to the pure Al can be ascribed to the coupled effects of (a) uniform distribution of nanosized reinforcement particles in the matrix and (b) enhanced dislocation density [31].

It can be noted that the compressive properties of the microwave-hot extruded Al-SiC nanocomposites are interestingly superior to that of conventional sintered AMMCs [9,10,32,33].

3.3.3. Tensile studies

Fig. 7(a) shows the typical engineering stress-strain curves of the microwave sintered and hot extruded pure Al and Al-SiC nanocomposites under tensile loading. It can be observed that, all extruded composites exhibited higher tensile strength in comparison to that of pure Al. The improved tensile strength of extruded composites is ascribed to the enhanced distribution of SiC nanoparticles. During extrusion, plastic deformation occurs in the metal matrix and hence the load is transferred to the hard reinforcement particles triggering the damage mechanisms related to the failure of the Al-SiC composite [34].

The average yield strength, ultimate tensile strength, and ductility values of the extruded composites as a function of added SiC particles are shown in Fig. 7(b) and Table 3. According to the results, the tensile yield strength (TYS) and ultimate tensile strength (UTS) of the composites gradually increases while % elongation decreases with the increasing of vol% of hard SiC particles. This observation can be attributed to the progressive increase in particle related damage events under the application of tensile loading [35]. However, tensile properties of the microwave-hot extruded Al-SiC nanocomposites are interestingly superior to that of conventional sintered AMMCs [29,32,34–36].

3.3.3.1. Strengthening mechanism analysis. Several mechanisms and theories have been recommended to elucidate the strengthening of metal matrix composites. However, the strength of the composites does not depend on a unique mechanism but several mechanisms may act simultaneously. These include Orowan strengthening, strengthening due to grain refinement, strengthening due to the formation of internal thermal stress resulted from different co-efficient of thermal expansion

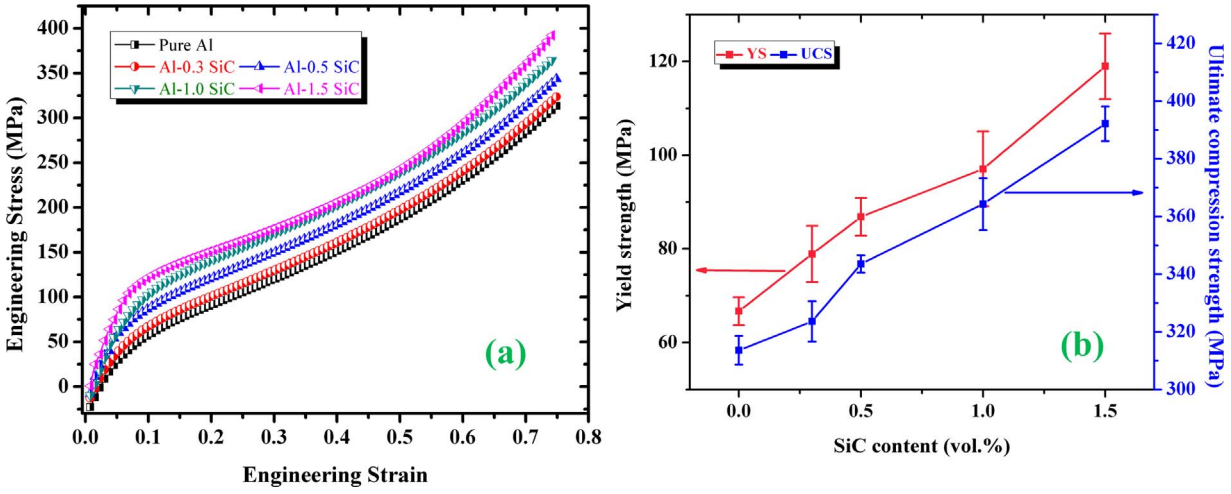

Fig. 6. Compression engineering stress–strain curves (a) and strengths (b) of microwave-hot extruded Al-SiC nanocomposites with different volume fraction of SiC particles.

Table 2
Compression behavior of Al–SiC nanocomposites produced by different techniques.

Material	Preparation method	Yield strength (MPa)	Ultimate compressive strength (MPa)	Failure strain (%)
Pure Al		66 ± 3	313 ± 5	> 75
Al–0.3vol%SiC	Microwave sintering	78 ± 6	323 ± 7	> 75
Al–0.5vol%SiC	+ Hot extrusion	86 ± 4	342 ± 3	> 75
Al–1.0vol%SiC		97 ± 8	364 ± 9	> 75
Al–1.5 vol% SiC	[Present study]	114 ± 7	392 ± 6	> 75
Al–25 wt%SiC [9]	Spark plasma sintering	–	315	–
Al–25 wt%SiC [10]	Conventional stir casting	–	72	–
Al–15 wt%SiC [32]	Hot press + Extrusion	143.2	210	–
Al–10 wt%SiC [33]	Casting technique	71	132	–

(CTE) values between the matrix and the reinforcement particles, strengthening due to the effective load transfer between the matrix and the reinforcement and the hardening due to the strain misfit between the reinforcing particulates and the matrix. In the present study, the strengthening mechanisms will be discussed from two points of view: (a) dispersion strengthening mechanism and (b) an increased dislocation density arising from a thermal mismatch between the matrix and reinforcement.

The strengthening mechanism resulting from dispersion hardening is known as Orowan strengthening. Orowan strengthening is expected to be the main active particle strengthening mechanism in the present metal matrix composites. The SiC nanoparticles prevent the movement of dislocations in the pure aluminum matrix through dispersion strengthening mechanism as given by the Orowan–Ashby equation [37].

$$\sigma_{Orowan} = \frac{0.13Gb}{\lambda} \ln \frac{r}{b} \tag{2}$$

where, G is the shear modulus of Al (68 GPa); b is the Burgers vector of Al (0.32 nm); r is the average radius of nanoparticles respectively. The interparticulate distance between the reinforcement particles within the Al metal matrix is given by equation [38]:

$$\lambda = \frac{4(1-f)r}{3f} \tag{3}$$

where λ is the distance between the reinforcement particles, f is the volume fraction of the reinforcement particles, and r is the particle radius.

According to Eq. (3), increasing the amount of SiC leads to a decrease in the distance between the SiC particles. By reducing the distance between the SiC particles according to Eq. (4) will result into an increase in the required compressive/tensile stress for the movement of dislocations between the SiC particles resulting into to an increase in the material strength.

$$T_0 = \frac{Gb}{\lambda} \tag{4}$$

In Eq. (4), T_0 is the required compressive/tensile stress for forcing dislocations to move among reinforcement particles. G is the elastic modulus of the matrix and reinforcement materials and b is the Burger's vector.

By minimizing the interparticulate distance, the tensile stress required for moving the dislocations among the reinforcement particles also increases, results in an increase of the composite strength. This observation supports the measured hardness values mentioned earlier.

In addition, the increase in ultimate tensile strength can also be attributed to the mismatch in CTE values of Al and SiC particles which contributes greatly to the high dislocation density and subsequent strengthening of the composite. In Al-SiC nanocomposites, there is a large difference in the thermal expansion coefficient (CTE) between matrix (24×10^{-6}/K for Al) and reinforcement (4.3×10^{-6}/K for SiC). Even small temperature changes can generate thermal stresses in the aluminum matrix. These stresses can be partially released by dislocation generation in the vicinity of the interface. Thus, the dislocation density generated can be quite significant at the interface and can be predicted using the model of Taya and Arsenault [39] based on prismatic punching of dislocations at a ceramic particulate.

$$\rho = \frac{B\varepsilon V_r}{bd(1-V_r)} \tag{5}$$

where, B is a geometric constant, ε is the thermal mismatch, V_r is the volume fraction of the reinforcement, b is the Burgers vector, and d is the average grain diameter of reinforcements.

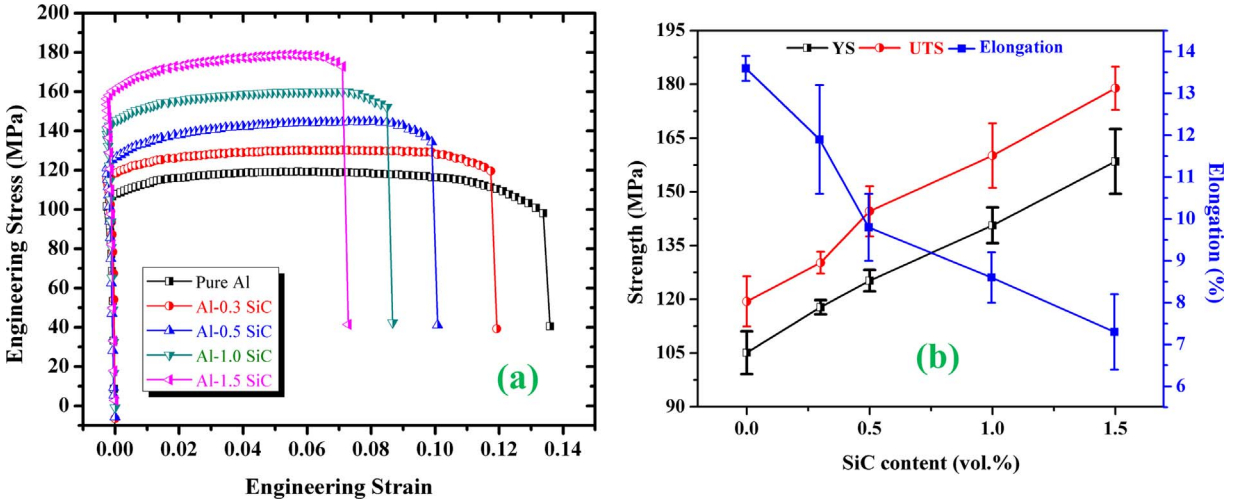

Fig. 7. Tension engineering stress–strain curves (a) and strengths, elongation (b) of microwave-hot extruded Al-SiC nanocomposites with different volume fraction of SiC particles.

Table 3
Tensile properties of Al–SiC nanocomposites produced by different techniques.

Material	Preparation method	Yield strength (MPa)	Ultimate tensile strength (MPa)	Ductility (%)
Pure Al		105 ± 6	119 ± 7	13.6 ± 0.3
Al–0.3vol%SiC	Microwave sintering	117 ± 2	130 ± 3	11.9 ± 1.3
Al–0.5vol%SiC	+ Hot extrusion	125 ± 3	144 ± 7	9.8 ± 0.8
Al–1.0vol%SiC		140 ± 5	160 ± 9	8.6 ± 0.6
Al–1.5vol%SiC	[Present study]	158 ± 9	178 ± 6	7.3 ± 0.9
Al–25 wt%SiC [10]	Conventional stir casting	82	88.46	5.0
Al–15 wt%SiC [32]	Liquid state mixing technique	130	167	7.2
Al–30vol%SiC [34]	Powder metallurgy + Hot extrusion	123	192	4.0
Al–2 wt%SiC [35]	Steering hot method	43.68	47	5.9
Al–15vol%SiC [37]	Casting technique	–	94.21	5.57

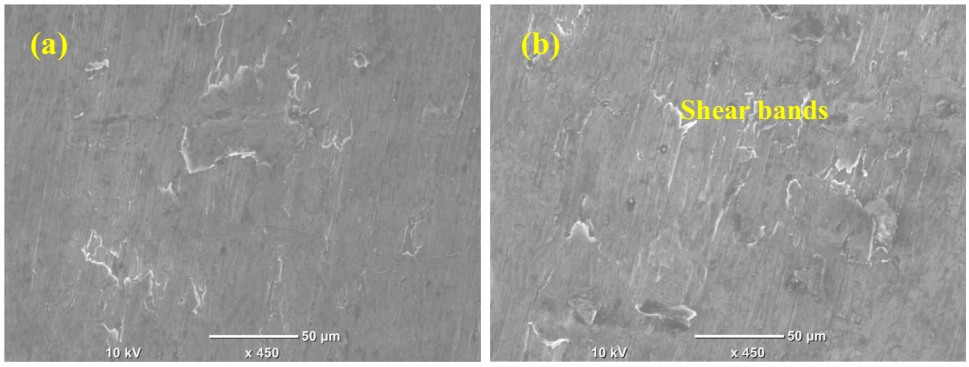

Fig. 8. SEM fractographs of (a) Pure Al and (b) Al-1.5 vol% SiC under compressive loading.

3.3.4. Fracture behavior

The fracture morphology analysis of extruded pure Al and Al-SiC nanocomposites tested under compression and tensile loading are shown in Figs. 8 and 9. The fractured compressive samples reveal a crack at 45° to the test axis. Fig. 8(a and b) clearly show shear mode fracture in both pure Al and Al-1.5 vol% SiC composite which also confirms that the compressive deformation of the developed Al-composites is significantly indifferent. This is due to heterogeneous deformation and rate of work hardening behavior [40].

Fractography of the fractured tensile test specimens reveals that the required bonding between powder particles could be obtained at the extrusion temperatures used in the present work, as no sign of primary particle boundary separation was observed at the fracture surface, even for specimens extruded at 350 °C, as shown in Fig. 9(a and b). Apparently, all the fractured surfaces revealed dimple like features indicating the degree of material's plasticity which can be correlated to the observed failure strain of more than 7% (see Table 3). The presence of SiC particles in the dimple cores and walls suggests that the fractured particles and agglomerates are potential stress concentration sites and susceptible to void formation. However, the presence of excellent interfacial integrity between the matrix and particles suggests an effective transfer of load between the soft aluminum and the hard SiC particles.

3.3.5. Nanoindentation studies

The load-displacement plots from nanoindentation for the extruded pure Al and Al-SiC nanocomposite samples are presented in Fig. 10(a). A maximum load of 100 mN was applied, and the indentation depth resides within 1.3–2.4 nm. Lower depth of penetration in composites can be observed from the nanoindentation graphs in comparison to that of pure Al. The decrease of indentation depth with the increase in hardness that agrees with the fact that hardness has been increased with increase in volume fraction of SiC particles. A similar trend in the hardness values was observed in the Al-TiC composites [41]. The lower displacement is attributed to the higher resistance offered by the matrix incorporated with hard SiC particles to the indenter.

The Young's modulus and hardness of extruded pure Al and Al-SiC composite samples achieved directly from the nanoindentation test, as shown in Fig. 10(b). The Young's modulus and hardness are observed to increase with increasing amount of hard SiC particles. The enhanced modulus for the extruded composites from 73.19 to 92.25 GPa by increasing SiC from 0 vol% to 1.5 vol% is attributed to the efficient load

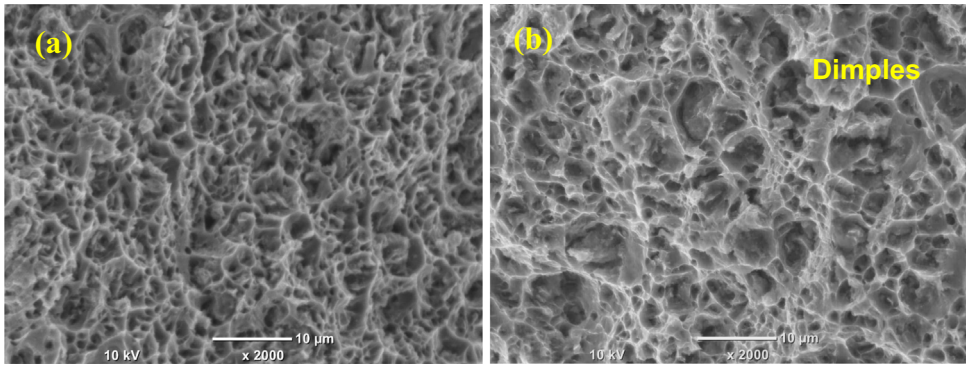

Fig. 9. SEM fractographs of (a) Pure Al and (b) Al-1.5 vol% SiC under tensile loading.

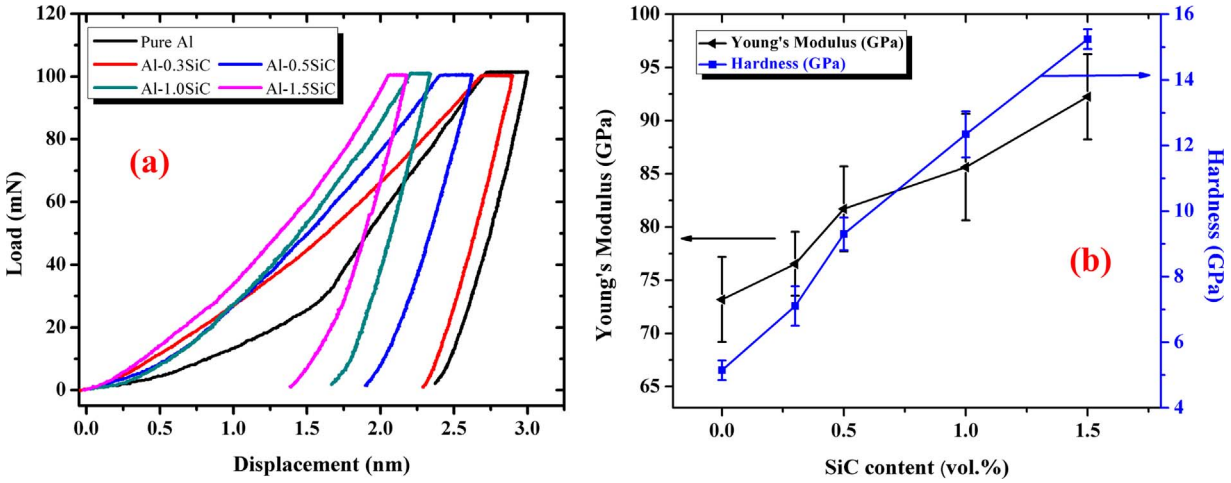

Fig. 10. (a) Room temperature load/unload–displacement curves and (b) Young's modulus and hardness of microwave-hot extruded Al-SiC nanocomposites.

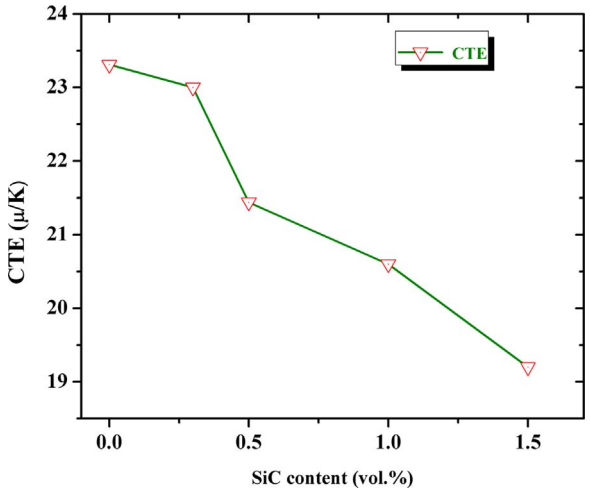

Fig. 11. The variation of CTE of microwave-hot extruded Al-SiC nanocomposites.

transfer across the ceramic-metal interface. The hardness was found to increase from 5.16 to 15.24 GPa with increasing of SiC content. Al-1.5 vol% SiC exhibited the maximum young's modulus and hardness value of 92.25 GPa and 15.24 GPa, which are ~ 26% and ~ 172% greater than that of pure Al. A similar increase of Young's modulus and hardness values also observed for 5 and 10 wt% of SiC using planetary ball mill and conventional sintering [41,42]. However, this increase in hardness is due to the uniform distribution of nano-sized reinforcement particles in the Al matrix and good interfacial bonding between matrix and reinforcement particles [43].

3.4. Coefficient of thermal expansion (CTE) of extruded Al-SiC nanocomposites

The measured CTE values are shown in Fig. 11. It can be observed that, the CTE values decreases with increasing volume content of SiC particles. It is in accordance with the theory that the thermal expansion of composites is governed by the competing interactions of expansion of Al matrix and the constraint of SiC particles through their interfaces [44]. The CTE of pure Al was measured to be 23.31×10^{-6} /K which is in close agreement with the theoretical CTE of aluminum (24×10^{-6}/K). The addition of 1.5 vol% SiC nanoparticles to Al reduced the CTE value to ~ 19.2×10^{-6}/K. This considerable decrease in CTE values may be the result of the addition of thermally stable SiC particles with CTE of 4.3×10^{-6}/K. CTE values in the present study are in agreement with those found from the literature; from 23.8×10^{-6} /K to 13.6×10^{-6} /K for SPS consolidated SiCp/Al composites [45]. The linear decrease in CTE values with the addition of SiC particles results in thermally stable composites and highlights the pronounced effect of SiC in improving the dimensional stability of Al. With Al being a leading material in aerospace and automotive industry, better dimensional stability at elevated temperatures becomes an important property for the application of any material.

4. Conclusions

In the present work, nano-sized SiC (0.3, 0.5, 1.0 and 1.5 vol%) particles reinforced aluminum metal matrix nanocomposites were successfully fabricated through microwave sintering process followed by hot extrusion. XRD, SEM and EDS analysis reveals the presence of Al and SiC components in developed composites. Under compression testing, the CYS and UCS values increased from 66 and 313 MPa for pure Al to about 119 and 392 MPa with the addition of 1.5 vol% SiC, respectively, which are ~ 80% and ~ 25% greater than that of pure Al. Under tensile testing, the TYS and UTS values increased from 105 and 119 for pure Al to about 158 and 178 MPa respectively, which are ~ 51% and ~ 49% greater than the pure Al. Ductility, however, decreased from 13.6% for pure Al to about 7.3%, which is ~ 46% lesser than the pure Al. The shear band and dimple formations were observed in Al-1.5 vol% SiC nanocomposites under compression and tensile loading, respectively. Young's modulus and hardness values of Al-matrix increased by increasing amount of SiC nanoparticles. Coefficient of thermal expansion values decreased with increased amounts of SiC particles indicating high dimensional stability.

Acknowledgments

This publication was made possible by NPRP Grant 7–159-2-076 from Qatar National Research Fund (a member of the Qatar Foundation). Statements made herein are solely the responsibility of the authors.

References

[1] V.S. Aigbodion, S.B. Hassan, J. Mater. Sci. Eng. A 447 (2007) 355–360.
[2] E.M. Sharifi, F. Karimzadeh, M.H. Enayati, Mater. Des. 32 (2011) 3263–3271.
[3] M. Penchal Reddy, F. Ubaid, R.A. Shakoor, P. Gururaj, M. Vyasaraj, A.M.A. Mohamed, M. Gupta, Mater. Sci. Eng. A 696 (2017) 60–69.
[4] E. Ghasali, A. Pakseresht, A. Rahbari, H. Eslami-shahed, M. Alizadeh, T. Ebadzadeh, J. Alloy Compd. 666 (2016) 366–371.
[5] K. Shirvanimoghaddam, H. Khayyam, H. Abdizadeh, M.K. Akbari, A.H. Pakseresht, E. Ghasali, M. Naebe, Mater. Sci. Eng. A 658 (2016) 135–149.
[6] M. Penchal Reddy, F. Ubaid, A. Shakoor, A.M.A. Mohamed, W. Madhuri, J. Sci: Adv. Mater. Dev. 1 (2016) 362–366.

[7] A.W. Weimer, Carbide, Nitride and Boride Materials Synthesis and Processing, First ed., Chapmann & Hall, London, 1997.
[8] S. Jayalakshmi, M. Gupta, Metallic Amorphous Alloy Reinforcements in Light Metal Matrices, Springer, London, 2015.
[9] L.Y. Chen, J.Q. Xu, H. Choi, M. Pozuelo, X. Ma, S. Bhowmick, J.M. Yang, S. Mathaudhu, X.C. Li, Nature 528 (2015) 539–543.
[10] Q. Zhang, G. Chen, G. Wu, Z. Xiu, B. Luan, Mater. Lett. 57 (2003) 1453–1458.
[11] M. Penchal Reddy, A. Shakoor, A.M.A. Mohamed, M. Gupta, Metals 6 (2016) 1–19.
[12] H.M. Zakaria, Ain Shams Eng. J. 5 (2014) 831–838.
[13] V.K. Singh, S. Chauhan, P.C. Gope, High. Temp. Mater. Proc. 34 (2) (2015) 163–170.
[14] D. Garbiec, M. Jurczyk, Compos. Theory Pract. 13 (2013) 255–259.
[15] O. El-Kady, A. Fathy, Mater. Des. 54 (2014) 348–353.
[16] H. Bian, Y. Yang, Y. Wang, W. Tian, H. Jiang, Z. Hu, W. Yu, J. Mater. Sci. Technol. 29 (5) (2013) 429–436.
[17] M. Gupta, W.L.E. Wong, Mater. Charact. 105 (2015) 30–46.
[18] C. Tekmen, I. Ozdemir, U. Cocen, K. Onel, Mat. Sci. Eng. A Struct. 360 (2003) 365–371.
[19] U. Cocen, K. Onel, Comp. Sci. Technol. 62 (2002) 275–282.
[20] Y.H. Seo, C.G. Kang, Comp. Sci. Technol. 59 (1999) 643–654.
[21] P. Gururaj, V. Manakari, M. Ganesh Kumar, M. Gupta, Inter. J. Mater. Res. 107 (2016) 1091–1099.
[22] C. Sun, M. Song, Z. Wang, Y. He, J. Mater. Eng. Perform. 20 (2011) 1606–1612.
[23] N. Chawla, J.J. Williams, R. Saha, J. Light Met. 2 (4) (2002) 215–227.
[24] W.L.E. Wong, M. Gupta, Tech 3 (2015) 1–18.
[25] T. Huber, H. Degischer, G. Lefranc, T. Schmitt, Compos. Sci. Technol. 6 (2006) 2206–2217.
[26] K. Chu, C. Jia, W.S. Li, Mater. Sci. Techonologies 28 (2) (2013) 1397–1401.
[27] S.A. Khadem, S. Nategh, H. Yoozbashizadeh, J. Alloy Compd. 509 (2011) 2221–2226.
[28] R. Roy, D. Agrawal, J. Cheng, M. Mathis, Ceram. Trans. 80 (1997) 3–26.
[29] M.H. Rahman, H.M.M. Rashed, Procedia Eng. 90 (2014) 103–109.
[30] L. Zhang, H. Xu, Z. Wang, Q. LiJunyan, J. Alloy. Compd. 678 (2016) 23–30.
[31] L.C. Davis, C. Andres, J.E. Allison, Mater. Sci. Eng. A 294 (1998) 40–45.
[32] M. Zakeri, A. Vakili-Ahrari Rudi, Mater. Res. 16 (5) (2013) 1169–1174.
[33] F. Shehata, N. ElMahallawy, M. Arab, M. Agwa, Open J. Metal. 3 (2013) 26–33.
[34] A. Pakdel, H. Farhangi, Conference on advanced manufacturing processes and technologies Nov 2–5, 2008.
[35] M. Salehi, H. Farnoush, A. Heydarian, J.A. Mohandesi, Metall. Mater. Trans. 46 (2015) 20–29.
[36] S. Kamrani, Z.R. Hesabi, R. Riedel, S.M.S. Reihani, Adv. Comp. Mater. 20 (2011) 13–27.
[37] G.E. Dieter, D. Bacon, Mechanical Metallurgy, McGraw-Hill, New York, 1986.
[38] A. Meyers, K.K. Chawla, Mechanical Behavior of Materials, Cambridge University Press, New York, 2009.
[39] M. Taya, R.J. Arsenault, Metal Matrix Composites – Thermomechanical Behavior, Pergamon Press, New York, 1989.
[40] D. Neelima, C. Mahesh, V. lvaraj, Int. J. Appl. Eng. Res. 1 (2011) 793–799.
[41] S. Mohapatra, A.K. Chaubey, D.K. Mishra, S.K. Singh, J. Mater. Res. Technol. 5 (2016) 117–122.
[42] P. Krizik, M. Balog, I. Matko, P.S. Svec, M. Cavojsky, F. Simancik, J. Comp. Mater. 50 (1) (2016) 99–108.
[43] L. Kollo, C.R. Bradbury, R. Veinthal, C. Jäggi, E.C. Morelli, M. Leparoux, Mater. Sci. Eng. A 528 (2011) 6606–6615.
[44] B. Anggara, S.B. Soegijono, KnE Eng. (2016) 1–5.
[45] Z. Ling, L. Luo, B. Dodd, J. Phys. IV 04 (1994) 453–458.